

Lattice design and 3D-printing of PEEK with $\text{Ca}_{10}(\text{OH})(\text{PO}_4)_3$ and *in-vitro* bio-composite for bone implant

Bankole I. Oladapo^{a,*}, Sikiru O. Ismail^b, Bowoto Oluwole^a, Francis T. Omigbodun^c, Matthew A Olawumi^a
Musa A. Muhammad^d

^a*School of Engineering and Sustainable Development, De Montfort University, Leicester, UK*

^b*Centre for Engineering Research, School of Physics, Engineering and Computer, University of Hertfordshire, England, UK*

^c*Mechanical Engineering, Loughborough University, UK*

^d*Faculty of Engineering, Environment and Computing, Coventry University Group, Scarborough, UK*

*Corresponding author, Tel: +44(0)1162013971, E-mail: P17243433@my365.dmu.ac.uk

Abstract

The addition of biomaterials such as Calcium hydroxyapatite (cHAp) and incorporation of porosity into poly-ether-ether-ketone (PEEK) are effective ways to improve bone-implant interfaces and osseointegration of PEEK composite. Hence, the morphological effects of nanocomposite on surfaces biocompatibility of a newly fabricated composite of PEEK polymer and cHAp for a bone implant, using additive manufacturing (AM) were investigated. Fused deposition modeling (FDM) method and a surface treatment strategy were employed to create a microporous scaffold. PEEK osteointegration was slow and, therefore, it was accelerated by surface coatings with the incorporation of bioactive cHAp, with enhanced mechanical and biological behaviors for bone implants. Characterization of the new PEEK/cHAp composite was done by X-ray diffraction (XRD), differential scanning calorimetry (DSC), mechanical tests of traction and flexion, thermal dynamic mechanical analysis (DMA). Also, the PEEK/cHAp induced the formation of apatite after immersion in the simulated body fluid of DMEM for different days to check its biological bioactivity for an implant. In-vivo results depicted that the osseointegration and the biological activity around the PEEK/cHAp composite were higher than that of PEEK. The increase in the mechanical performance of cHAp-coated PEEK can be attributed to the increase in the degree of crystallinity and accumulation of residual polymer.

Keywords: PEEK/cHAp; Biocompatible; Nanostructure; Bone implant.

1. Introduction

Biocompatible materials have been developed, and the great development and study on the use of these materials in contact with the human body can be dated from the 1960s [1-3]. Biomaterials must have an acceptable biological response to be called biocompatible. They do not cause significant damage to the structures adjacent to their application during the period of contact with the human body when they are used. One of the main applications of biomaterials is the orthopedic area. The applied biomaterial remains in contact with bone structures, usually under mechanical loading, to replace or assist in the regeneration of these structures. In this case, where the product manufactured with the biomaterial remains in contact with the human body, it is called an implant [4-6]. To this end, several material properties must be taken into account, such as biocompatibility, an acceptable biological response. Also, the mechanical properties must withstand mechanical stresses and the thermal properties must not present large differences in the coefficient of thermal expansion with the human body to avoid dimensional changes, which cause pain to the patient [7-9].

Metallic materials were the first to be used as implantable materials, especially stainless steel, titanium alloys, chromium-cobalt alloys, among others, due to their excellent mechanical properties of short and long durations, which meet the efforts related mechanics. However, some complications have been recorded with the use of these materials, due to the large difference in their elastic moduli and bone, causing the effect known as stress-shielding [10-12]. When using a material with a higher elastic modulus than that of human bone, the mechanical loading is transferred to the implant. Thus, there is a reduction in the application of mechanical loading of the adjacent bones, causing a reduction in the density of the same bones and later results in osteopenia. In this context, the use of polymeric materials with physical properties, such as density and thermal properties, expansion coefficient, and thermal and mechanical conductivity, as their elastic module are close to that of human bones, becomes a more attractive alternative to replace traditional metallic materials [13-15]. The use of polymeric materials in implantable applications began with the use of ultra-high molecular weight polyethylene (UHMWPE) in the 1970s. Its excellent wear resistance has made this polymer a biomaterial for application in hip prostheses, especially in the acetabular part, a particular part that suffers shear wear [16-18]. However, the femoral part of the prosthesis was still made of metal, since the mechanical loads in this region are very high, and the use of UHMWPE is not possible. Therefore, studies continued and produced manufacturing of prostheses with materials called isoelastic, that is, with a bone-like module that could withstand high levels of mechanical loading, even under fatigue. In an attempt to further this gap, some studies on **the use of polyaryl-ether-ketones started. In the 1980s, poly ether-ether-ketone (PEEK) had its biocompatibility potential for applications in biomedical [19-22].**

Therefore, this study focused on the influence of PEEK surface treatment with calcium hydroxyapatite (cHAp) on short and long-term mechanical behavior, intending to use this material as surgical implants. The main stages of experimental development were considered in this work, as evaluation of the processing conditions used, both with the processing of the fabricated implant and surface coating by injection, and fabricated PEEK polymeric composite coated with cHAp by surface coating technique. Mechanical and thermomechanical tests evaluated the processing parameters used and their results were compared with those reported in the current state-of-the-art literature. Evaluation of the efficiency of the PEEK surface treatment process by surface coating, using surface coat as well as its impact on its mechanical properties, through short-term mechanical tests on the polymeric composite were included. Also, other studies on surface coat treatment such as traction, flexion, dynamic mechanical analysis (DMA) and scanning electron microscopy (SEM), as well as analysis of the thermal shock effects on the crystalline morphology of the PEEK resin via differential scanning calorimetry (DSC) analysis were carried out.

2. Method and materials

Additive manufacturing (AM) was initially developed for industrial purpose, as a resource for the development of optimized and quality products [23-26]. However, with time, it has permeated several domains of knowledge, including the health area. It is used in the health field to aid diagnosis, plan complicated surgeries and as a tool in the construction of customized prostheses [27-29]. The set of two-dimensional (2D) images in the international standard format [30-32], relative to the different slice planes or slices of the body, is used in the reconstruction of the three-dimensional (3D) volume of the anatomical region of interest through particular imaging systems. Mountain 8 Premium software was used for the reconstruction of images from developed models available. The 3D virtual model was transformed into the stereolithography (STL) pattern to be interpreted by the AM equipment,

which was responsible for the construction of the physical prototype that effectively reproduced the anatomy of interest. Fig. 1. represents a process of design of lattice structure for bone implant in fused deposition modeling via *in vitro*. This physical model is called a bio-model in health-related applications [33-35]. In the subsequent processes, the polymer-rich phase becomes a matrix, and the polymer-lean phase turns into pores when the solvent gets evaporated.

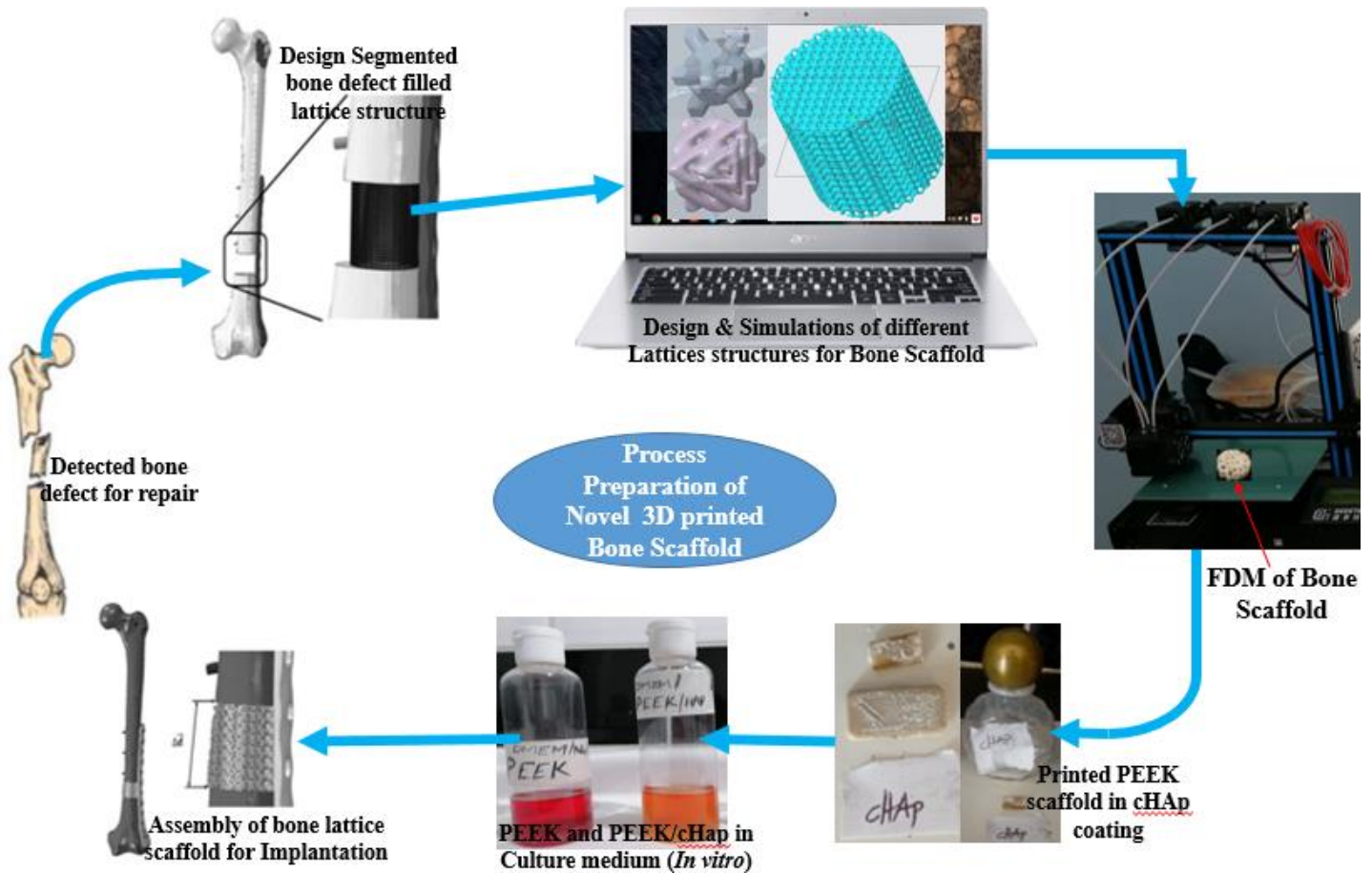


Fig. 1. process of a bone implant in fused deposition modeling via *in-vitro*.

The desired geometric shape of the final complex object was created under the control of a computer. The extrusion temperature was set at 380-410°C, and the printing speed was 40 mm/sec. The bead width of each print line was 0.4 mm, and the layer thickness was 0.2 mm (Tables 1 and 2). Also, the PEEK filler, which was a 3D printed material in this study, was reused from pellets of 5% carbon fiber with a length of 75-145µm and a diameter of 6.89µm in the composite materials were also chosen wast filament from the printed part was used.

Table 1

Principles and characteristics influencing parameter setting of the converted luminance of the tissue engineering 3D-printed scaffold.

ISO 25178: Height parameter		
	Functional parameter	
Areal material ratio (S _{mr})	0.112%	C = 0.001 under the highest peak
Inverse areal material ratio (S _{mc})	27	P = 10%
Extreme peak height (S _{xp})	27.9	P = 50%, q = 97.5%

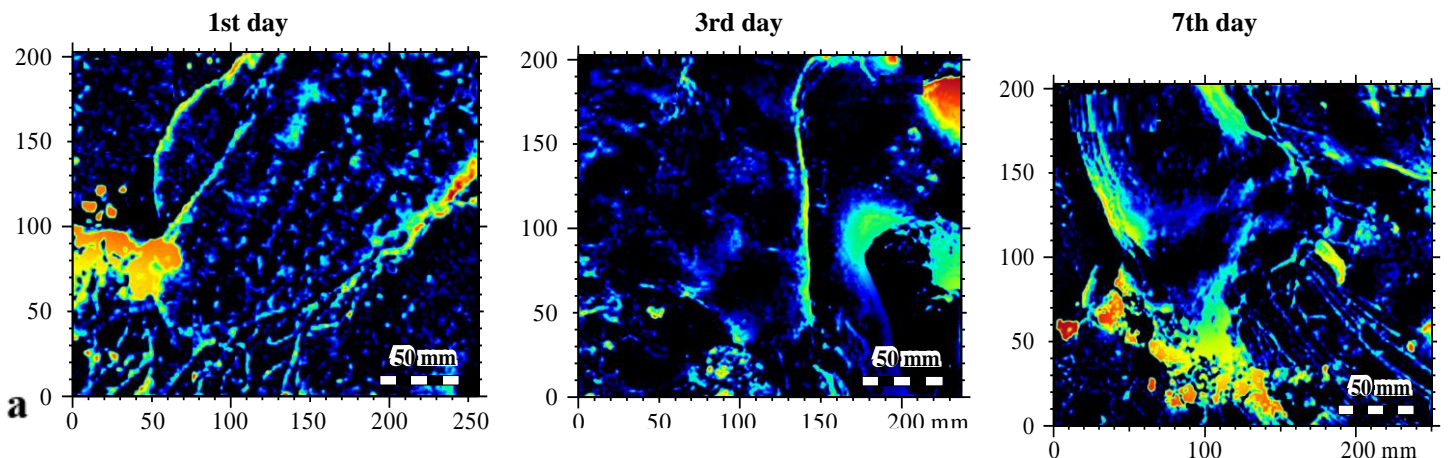
	Spatial parameters	
Autocorrelation length (Sal)	7.64 mm	S = 0.2
Texture-aspect ratio (Str)	0.765	S = 0.2
Texture direction (Std)	51.7°	Eference angle = 0°
	Hybrid parameters	
Root-mean-square gradient (Sdq)	62.6	
Developed interfacial area ratio (Sdr)	40.24%	
	Feature parameters	
Density of peaks (Spd)	0.102 mm ⁻²	Pruning = 5%
Arithmetic mean peak curvature (Spc)	373 mm ⁻²	Pruning = 5%

Table 2

Technical specifications and printing parameters of the FDM for the PEEK/cHAp.

Parameters	Technical specifications
Nozzle diameter	0.4 mm
Bed width	210 mm
Layer thickness	0.2 mm
Printing speed	45 mm/s
Raster angle	Longest edge
Ambient temperature	30°C
Chamber Temperature	90 oC
Bult Plate temperature	110-160°C
Nozzle temperature	350-410°C

According to the manufacturers, besides providing the physical bio-models directly from the biomaterials with high conformity to the virtual bio-models, the scaffolds equipment (3D printer) was constructed with the most varied geometries, dimensions [36-38]. Therefore, for surgical planning and training, the direct implant **technology for personalized implants can be passed on to the unified health system in the future**. Fig. 1 represents a process a study of nanostructure for osseointegration and biomechanical properties of the PEEK/cHAp scaffolds in tissue engineering. The slice luminance conversion of the nanoparticles and frequency luminance spectrum conversion of the micro-nanoparticle was set for the furrows luminance spectrum of a micro nanoparticle. The furrows **parameters value** was set to have a maximum depth of furrows of 81.07 nm, a mean depth of furrows of 29.22 nm at a mean density of furrows of 2.663 cm/cm² (Fig. 2).



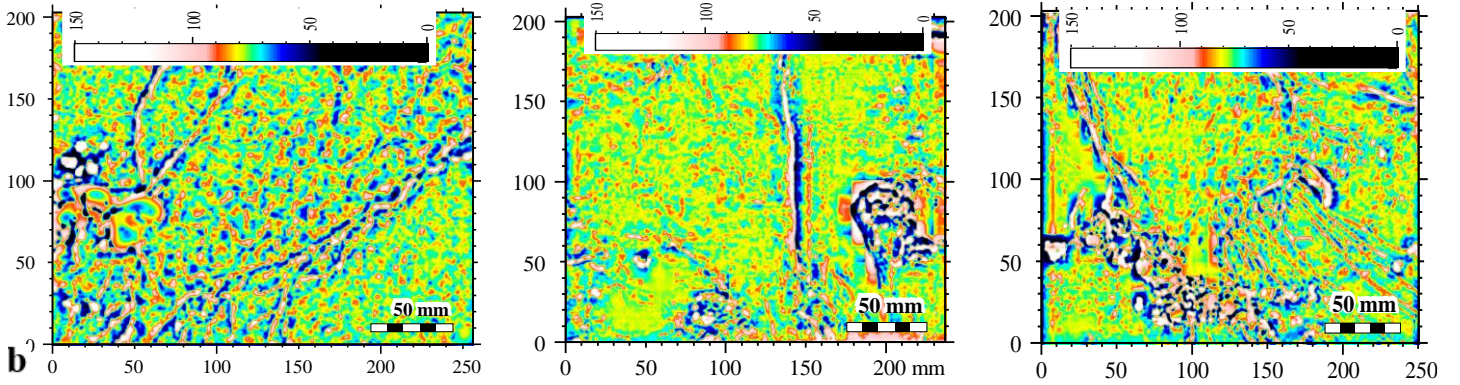


Fig. 2. The process of the study of osseointegration and biomechanical properties of the PEEK/cHAp scaffolds in tissue engineering, showing the (a) Surface converted luminance furrows luminance spectrum of micro-nanoparticle, scaled sample profile for analysis in the Gaussian filter of 0.8 mm and (b) roughness of the wavelet filter pf Daubechies slice luminance conversion of the nanoparticles.

3. Lattices of 3D nanostructure

In 3D printing, also known as AM, an object is built in layer-by-layer, allowing the creation of structures that would be impossible to manufacture with conventional subtraction methods, such as engraving or milling. Composite materials are one of the basic materials used in creating ultrafine 3D structures built through AM for a bone implant and, for example, built 3D lattices whose beams are only nanometers long and wide, too small to be seen with the naked eye. These materials exhibit unusual, often surprising properties and created exceptionally lightweight biocomposite that returns to their original shape after being compressed [40-43]. AM/3D printing was used to make porous PEEK with higher capacity and lower weight. Researchers have developed a new method for 3D-printed bone structure by creating a microreticule structure with controlled porosity. In the case of PEEK composite, structure with porous architectures can lead to higher inflow capacities of body fluid. The pore size, α was calculated based on the geometrical parameters of cell size, ζ and strut diameter, d for the cubic design, as expressed in Eqs. (1) and (2).

$$\alpha = \zeta - d \quad (1)$$

$$\text{For the diagonal design: } \alpha = \sqrt{2} \cdot \left(\frac{\zeta}{2} - d\right) \quad (2)$$

And for pyramidal design, Eqs. (3) and (4) were applied.

$$\alpha_1 = \frac{\sqrt{17}}{4} \cdot \zeta - d \quad (3)$$

$$\alpha_2 = \frac{\zeta}{2} - d \quad (4)$$

3.1. Scanning electron microscopy analysis

Scanning electron microscopy (SEM) was used to carry out image analysis at the life science laboratory, De Montfort University. Analyses of the integrity of the covered layer (layer morphology) before and after mechanical cycling, as well as analysis of parameters layers, such as thickness, morphology, presence or absence of cracks, roughness, and porosity, were done. The analyses were made on the coating surface and also on fractured flexion specimens, according to the ASTM D790 standard for analysis of their cross-sections of the fabricated specimen [44-47]. The specimen was fabricated after static bending with a cHAp tensile and comprehensive testing

experiment and a 90% flow deformation. X-ray diffraction was used to evaluate the surface coat process used to determine whether the obtained layer corresponds to the necessary and expected one for application as an osteoconductive layer. This analysis was made by comparing the X-ray diffraction spectrum obtained with the current state-of-the-art results obtained from the literature review. The DCS for determining the thermal shock effect of the coating process on polymer crystallinity was based on the evaluation of the thermal shock to which the PEEK specimens were exposed during the coating process. This exposure was to determine whether the crystallinity levels of the PEEK matrix were altered [48-50]. The analysis was focused on the superficial layers of the specimens, since these are the most susceptible to changes, due to the greater exposure both to the temperature field and the mechanical impact of the process. In particular, PEEK samples coated with cHAp had their mass removed just below the cHAp layer, minimizing the risk of cHAp particles interfering with the results.

All analyses were carried out using the TA Instruments DSC Q2000, differential scanning calorimetry, and modulated DSC, on the premises of the thermal analysis at De Montfort University laboratory of the polymer section of the materials engineering department. The analyses were performed twice. Also, software analysis for accurate results, such as DigitSurf (Mountain 8 Premium) Instrument, was used. The tensile test was performed on PEEK specimens with cHAp coated and uncoated according to ASTM D638 [51,52] to initially assess the impact of the presence of the cHAp layer on the mechanical strength under tension, as similarly reported [53-55]. The static tensile test for PEEK specimens was terminated after the specimen was fractured. This was not observed in the flexion test since the specimen deformed without breakage. Thus, when performing the static tensile test, it was possible to analyze the impact of the coating process, both on the tensile strength properties, resilience, and fracture toughness.

3.2. Cell culture and in-vitro cytotoxicity

The cells were cultured in Dulbecco's modified eagle medium (DMEM) pouch, low glucose, 5/pack supplemented with 10% fetal bovine serum, 1% penicillin/streptomycin and 1% GlutaMAX in 75 cm³ sterile cell culture flasks was purchase from USA. The medium was a basal medium for growing various types of mammalian cells. DMEM provided a fourfold enhancement of amino acids and vitamins in the original eagle's medium. The economical DMEM powder was easy to transport and store, having low glucose levels of 1 g/L with little or no NaHCO₃ and Phenol Red of L-glutamine without sodium pyruvate. The cells were cultured at 37°C in a humidified atmosphere of 4.98% Carbon dioxide. The culture medium was replaced every day. The formulation was 9.9 g of powder for 1 liter of DMEM medium. This was supplemented with 3.7 g sodium bicarbonate for every 1 liter of DMEM medium before use. One bag of powder of 15.25g was poured into a container, then deionized water was added to make the mix up to 450 mL and was stirred with a magnetic stirrer bar. The content was heated to promote the dissolution of the powder in water after adding deionized water to 0.5 L and was then autoclaved for 15-20 minutes at 121 °C. The solution was cooled down for it to be warm, and then antibiotics were added, and the mix was dispensed into sterile Petri dishes.

The cells were stored in an incubator in an atmosphere at 4.98% Carbon dioxide at 37°C. DMEM culture media were always renewed every four days. When the cells appeared, Fusion Trypsin was obtained from UK and used to separate them from the bottom of the flask, and 9.98% of all cells were put to a new container. PEEK and carbon fiber reinforced-PEEK extracellular toxicity tests were performed, using an extraction method according to ISO 10993-5 [32]. The cell was produced by adding moisture content to the sample with a DMEM cell at 37°C for

days. The ratio between the sample surface area and the extraction volume was $3\text{cm}^2/\text{mL}$. At the same time, the cells were pre-mixed for 24 hours. L929 was equal to 30,000 cells per centimeter square in $200\ \mu\text{L}$ of central DMEM per well in a 95.79 well sheet. After different days, the culture medium was removed from each cell and replaced with $145\ \mu\text{L}$ separately from the relevant sample (Fig. 3).

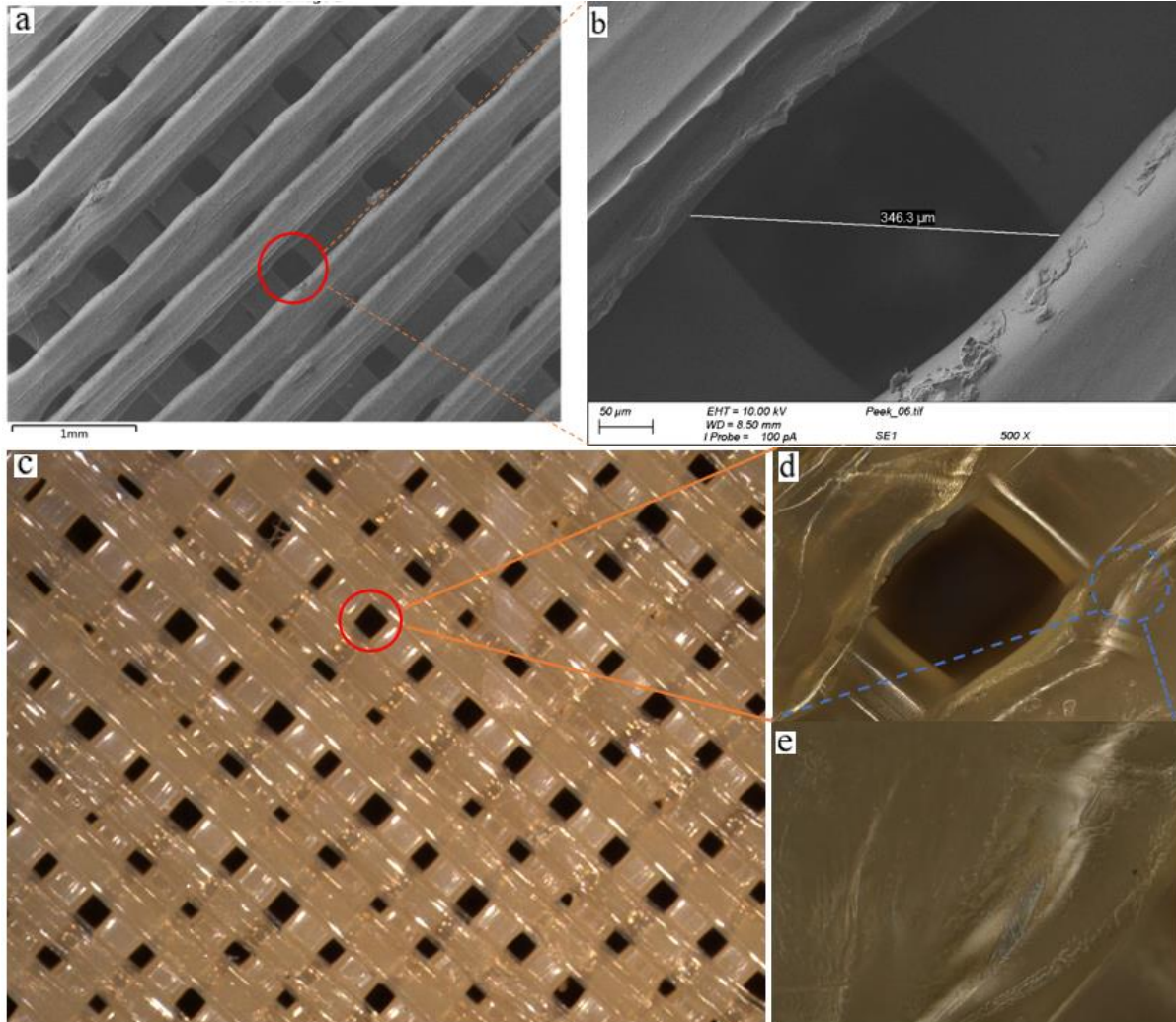


Fig. 3. SEM micrographs taken for a reference specimen, showing a significant development of cavities in the PEEK composite with porosity towards the center, due to the loss of the weight of the sample: (a) element are showing porosity and particle at 100x magnification, (b) $50\ \mu\text{m}$ magnification, (c) 100x magnification, (d) 500x magnification of a $712\ \mu\text{m} \times 534\ \mu\text{m}$ porosity material and (e) 1000x magnification of Pixel to Micron of 0.2225 in an exposure time of 1.2872 ms with a resolution of $0.2225\ \mu\text{m}/\text{Pixel}$.

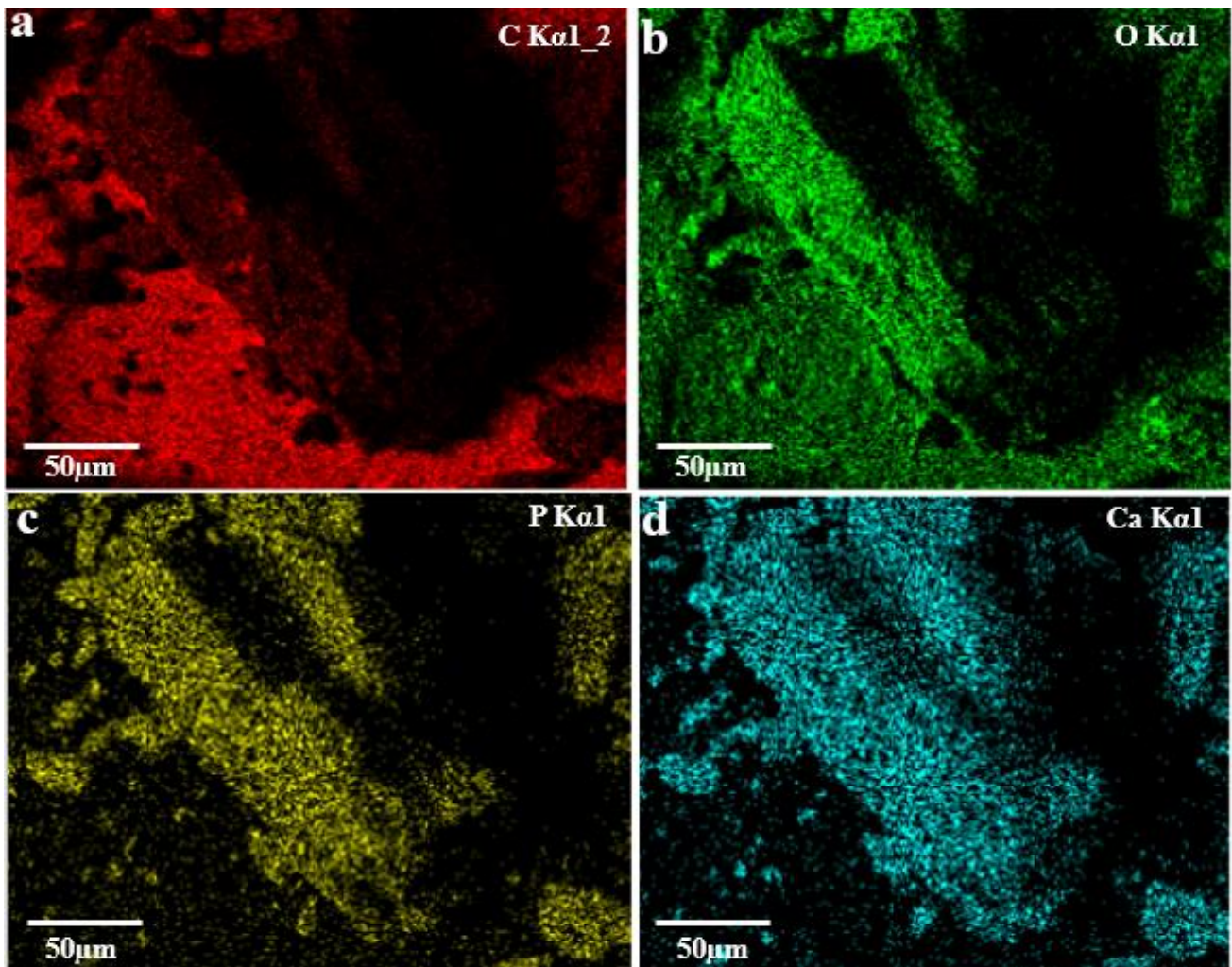
4. Results and discussion

Analyzing the particle morphology in the micrographs with a greater magnification of $10\ \mu\text{m}$, it was observed in the theoretical foundation that the particles with a circular profile presented a fusion of their ends, maintaining the solid center. Fig. 4 shows the SEM results obtained in the samples with particle morphology. As detailed in the methodology, to analyze the impact of mechanical stress on the adhesion of the coating layer, several mechanical samples were developed. Considering the sample surface as fabricated, a microfracture of an essentially fragile character was observed in its core with slight plastic deformation in the surface areas.

4.1. X-ray diffraction

Fig. 4(c) shows a standard X-ray diffraction spectrum for PEEK, in red color. The sample of PEEK/cHAp of opposite side 0.1 has a grain particle of 7.3 mg with a ramp method. There was an absolute difference of approximately 2% in the level of crystallinity between the skin exposed to the surface coating process with cHAp, when compared with the unexposed side. This behavior, albeit subtle, indicated a change in the level of crystallinity from the surface coat process. Then, the analysis was performed on the PEEK specimen only, subjected to the thermal shock process originating from the surface coat process, which presented the following results. The setting data obtained for crystalline fusion temperature (T_m) and crystallinity level (%) for PEEK samples were framed of 340 °C with 28.6%, respectively. The cHAp was exposed to treatment at a melting temperature crystalline value of 341 °C and a 30.5% level of a crystal, having a thermal shock exposed to 338 °C.

Moving forward, it is observed that the samples taken from the layers exposed to the surface coating process showed a slight increase in its level of crystallinity in the order of 2% in absolute terms and 10% in relative terms. Also, the result of the crystallinity level for samples only subjected to the thermal shock of the surface coating process was slightly higher than that of the crystallinity level of the sample coated with cHAp. It indicated that there was no interference of possible particles of cHAp in the samples taken, considering the methodology used in this study. It also minimized the need to perform a thermogravimetric analysis test (Fig. 4).



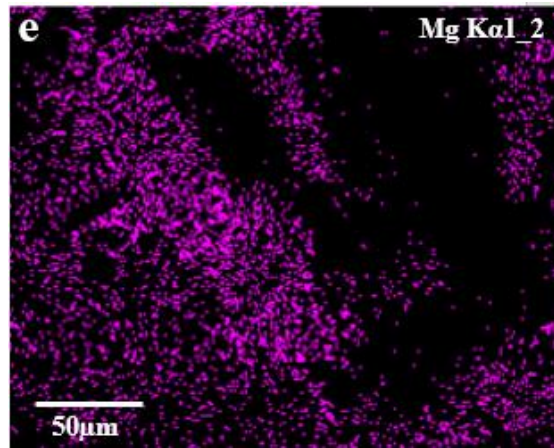


Fig. 4. Eletron layers of cHAp of Energy Dispersive X-Ray Spectroscopy (EDS) analysis (a) C K α 1_2(b) O K α 1 (c) P K α 1 (d) Ca K α 1 (e) Mg K α 1_2.

Various relevant tests were conducted to analyze the mechanical behaviors of the different specimens. The test involved an analysis of the tensile properties of PEEK and composite (Table 3). The stress-strain curve for the sample was later presented in Fig. 7(a). The amplitude of deformation was constant for the entire range of temperatures evaluated ($T_{amb} - 250^{\circ}C$). To expand the resolution of the results, in a second moment, the deformation amplitude was increased to 60 μm . The similarity in the aspects of the curves of storage module (E'), loss module (E''), loss tangent ($\tan \delta$), and strain range for both levels of strain used 20 and 60 μm . From the analysis, it was also observed that the values of E' were in line with those presented by [40-43] for all temperature ranges, showing a peak of $\tan \delta$ (T_g) at temperatures of the order 150-160 $^{\circ}C$. Thus, it was possible to define the amplitude of 60 μm for the other analyzes concerning this study to obtain the best possible resolution.

Table 3

Static tensile and static flexion test results of PEEK composite.

Properties	Flow tension (MPa)	Flow deformation (%)	Breaking stress (MPa)	Fracture deformation (%)	Modulus of elasticity (GPa)
Static tensile test					
Mean value	95.05	3.78	97.08	24.29	3.4
Standard deviation	0.98	0.15	0.80	1.57	0.08
Static flexion test					
Mean value	127.37	4.10	139.10		3.6
Standard deviation	1.82	0.059	4.95		0.059

To guarantee the reproducibility of the results, because there were superficial changes that caused sensitive changes, three samples in thermal shock conditions (Fig. 5), those with the greatest source of variability, were performed and compared with the property of E' . After the stage of coating the specimens, the analysis was carried out using the same test parameters previously defined as the specimens after cHAp coated to PEEK. All evaluations were carried out in duplicate or triplicate, with the median curves always presented. In the case of outliers, they were disregarded. 3D printing structures from a variety of materials: ceramic to organic compounds have been difficult to print, especially when it comes to creating structures less than about 50 microns in size, or approximately half the width of a human hair. Nanoscale 3D printing was done through a high precision laser that

exited the liquid at specific locations in the material with just two photons or light particles. This provided enough energy to harden liquid polymers into solids, but not enough to fuse metals. PEEK may not respond to light in the same way as the polymeric resins used to make nanoscale structures. There was a chemical reaction that was triggered when light interacted with a polymer. This hardened it and then formed a particular of cHAp in PEEK; this process was fundamentally impossible. A solution on organic bonds and molecules that adhered to materials to create a resin that contained mostly polymer, but carried with it a printable metal, such as scaffolding in the experiment described in the organic molecules together was employed to create a liquid that closely resembled bone implant. A designed structure using computer software, and then built it by 'zapping' the liquid with a two-photon laser was done. The laser creates stronger chemical bonds between organic molecules, hardening them into building blocks for the structure.

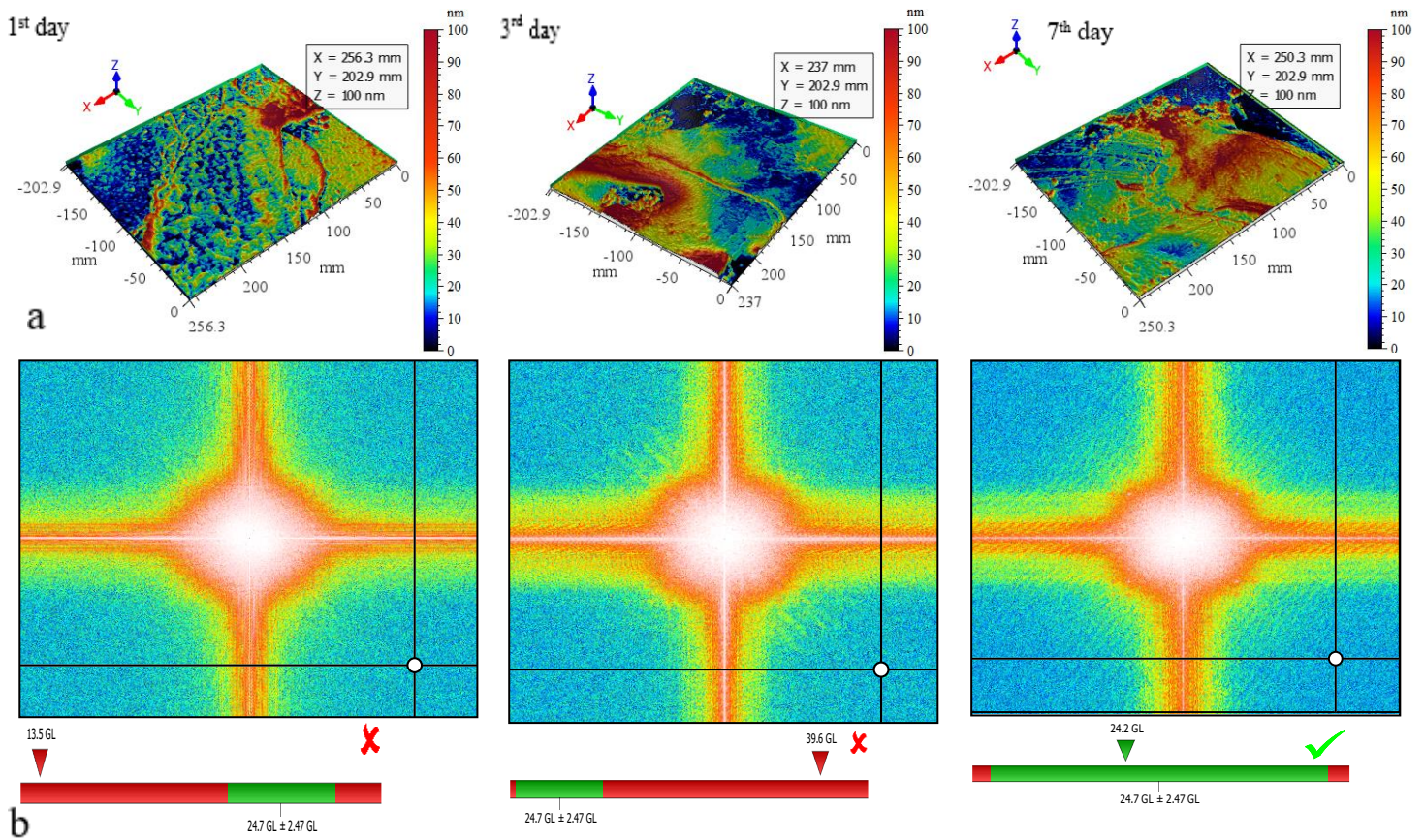


Fig. 5. (a) Binarized grains analysis result after segmentation of hill detection of the PEEK/cHAp in 3D view and (b) frequency spectrum and tolerance limit test from the sample of reduced valley depth (S_{ck}) of luminance of particles of the grains analysis result for PEEK/cHAp in grain/mm².

Therefore, it is possible to conclude that the cHAp coating process caused a thermal shock effect on the PEEK, increased the level of surface crystallinity, and consequently, the level of elastic response in the glassy regime, inducing an increase in the level of frozen stresses in the polymer. When the glass transition temperature was reached, these stresses were relaxed, with the cHAp layer functioning as an anchoring point, preventing such relaxation from occurring at higher levels. It can be verified by the $\tan \delta$ value, slightly lower for samples effectively coated with cHAp when compared to thermal shock only. The results observed for the E' also corroborated this fact, since the highest value of E' in the viscoelastic regime was recorded for the sample only to thermal shock, followed by the PEEK/cHAp samples without mechanical damage after static bending, with the

sample as-fabricated showing the lowest value for this property. This behavior demonstrated the effect of the higher level of crystallinity obtained for the sample subjected to thermal shock and cHAp treatments. DMA tests after mechanical cycling for 106 cycles in samples subjected to the surface coating and in samples coated with cHAp demonstrated different behaviors when compared with samples in the same conditions without mechanical stresses, as shown in Table 4. These phenomena can be viewed as quantitatively. Tabulating the data for three reference temperatures for the parameters of E' , E'' and $\tan \delta$, as shown in Figs. 6(a)-(c), respectively.

Table 4

Results of the DMA test post mechanical cycling of viscoelastic regime.

Sample	Max. temperature of $\tan \delta - T_g$ ($^{\circ}\text{C}$)	Intensity of $\tan \delta$ ($^{\circ}\text{C}$)
PEEK 106-cycle fatigue	161.7	0.207
cHAp	161.2	0.205
PEEK/cHAp 106-cycle fatigue	159.9	0.205
PEEK thermal shock	164.4	0.223
Fabricated propertie	165.0	0.194

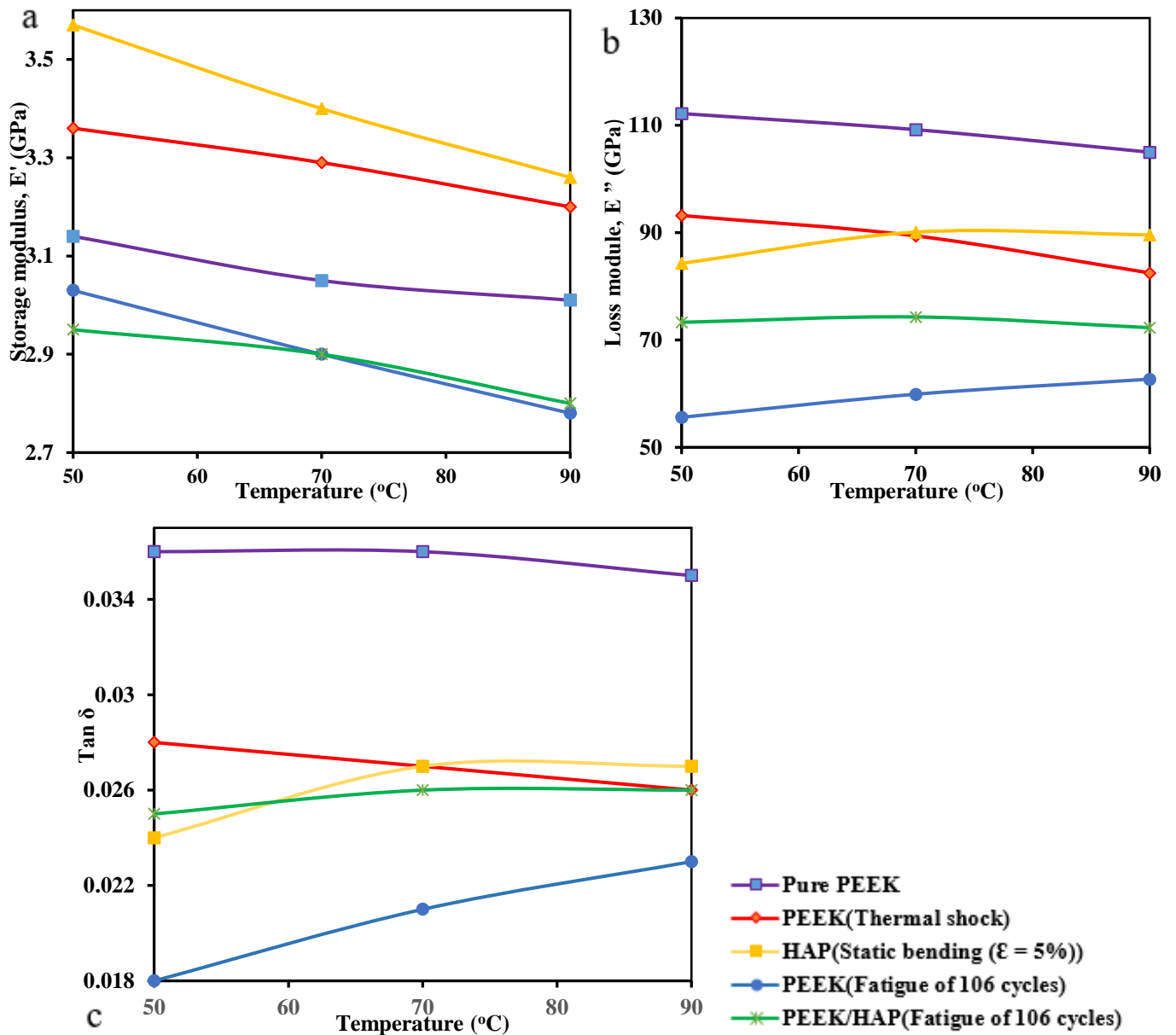


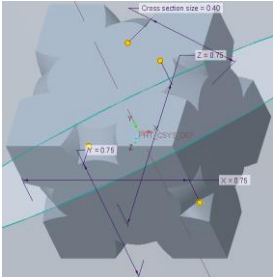
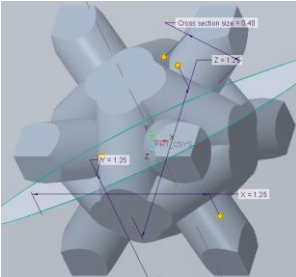
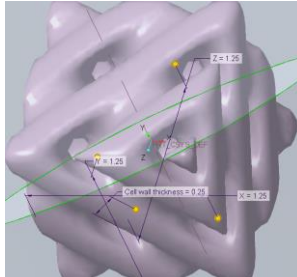
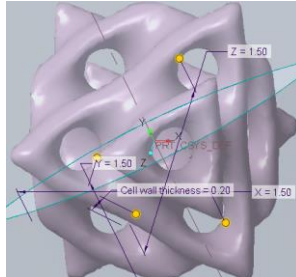
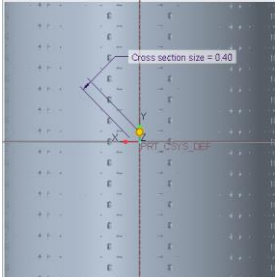
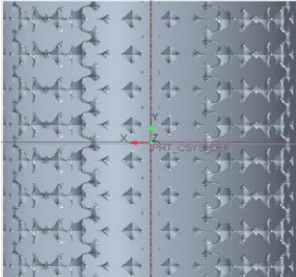
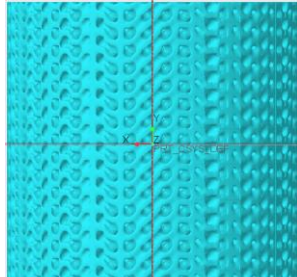
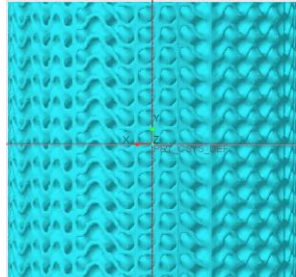
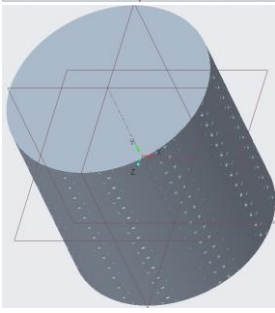
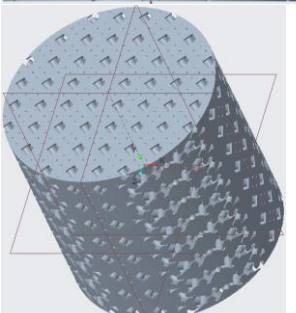
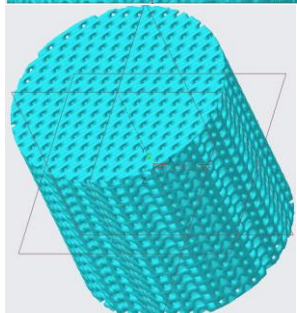
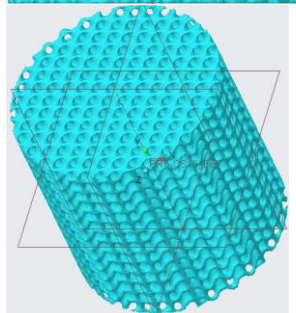
Fig. 6. Results of the DMA test and post mechanical cycling of the elastic region of the samples, showing
(a) E' , (b) E'' and (c) $\tan \delta$.

4.1. Lattices structure

The cell retained their complex 3D lattice structures after forty cycles, which demonstrated their mechanical robustness. Therefore, bone can have a large capacity for the same weight or the same size, a deficient pressure, and an essential attribute for body fluid transport applications. This revolutionary method is critically relevant to a cell and the medical device industry applications. The study integrates well with biomedical cell devices, where miniaturized scaffolds are required [33-35]. The microdevices, a non-biological cell, will also benefit from this work. And on a larger scale, a bone implant can also use this technology, due to the low weight and high capacity of batteries printed with this method. The lattice structure of the 3D printing scaffold in Face Center Cubic (FCC) Octahedron and diamond of cell diameter of 0.4mm of FCC-Octahedron and two cells of 0.25 and 0.2mm for diamond structure. (Table 5)

Table 5

Different lattice structures for the 3D printing of Scaffold

Lattices Type	FCC-Octahedron		Diamond	
Cell	0.75 x 0.4	1.25 x 0.4	1.25 x 0.25	1.5 x 0.20
Δ Vol.(mm ²)	0.0231	0.2306	0.2757	0.4332
Vol. (mm ²)	0.7623	0.5548	0.5097	0.3522
% Porosity	2.95%	29.36%	35.10%	55.16%
Unite Cell				
Face Structure of Lattices (10x10mm)				
3D View				

Also, Fig. 7 presents information on the zoom factor from SEM of four times and non-smoothing with 180 degrees for the 180 angular profiles, producing a spatial frequency and amplitude of 0.116 mm^{-1} and 658 GL^2 , respectively for the first day, 0.111 mm^{-1} and 729 GL^2 for the third day and, 0.108 mm^{-1} and 7178 GL^2 for the seventh day. The resultant dominant spatial frequency and maximum amplitude of the first, third, and seventh days were 0.0144 mm^{-1} and 7000 GL^2 , 0.013 mm^{-1} and 7987 GL^2 , and 0.0124 mm^{-1} and 7822 GL^2 , respectively. The sample subjected to 90% of the tensile flow resistance demonstrated that the layer remained well adhered to the PEEK surface, even after a high level of static deformation, showing no detachment. This can be observed by comparing Figs. 7(a) – (d).

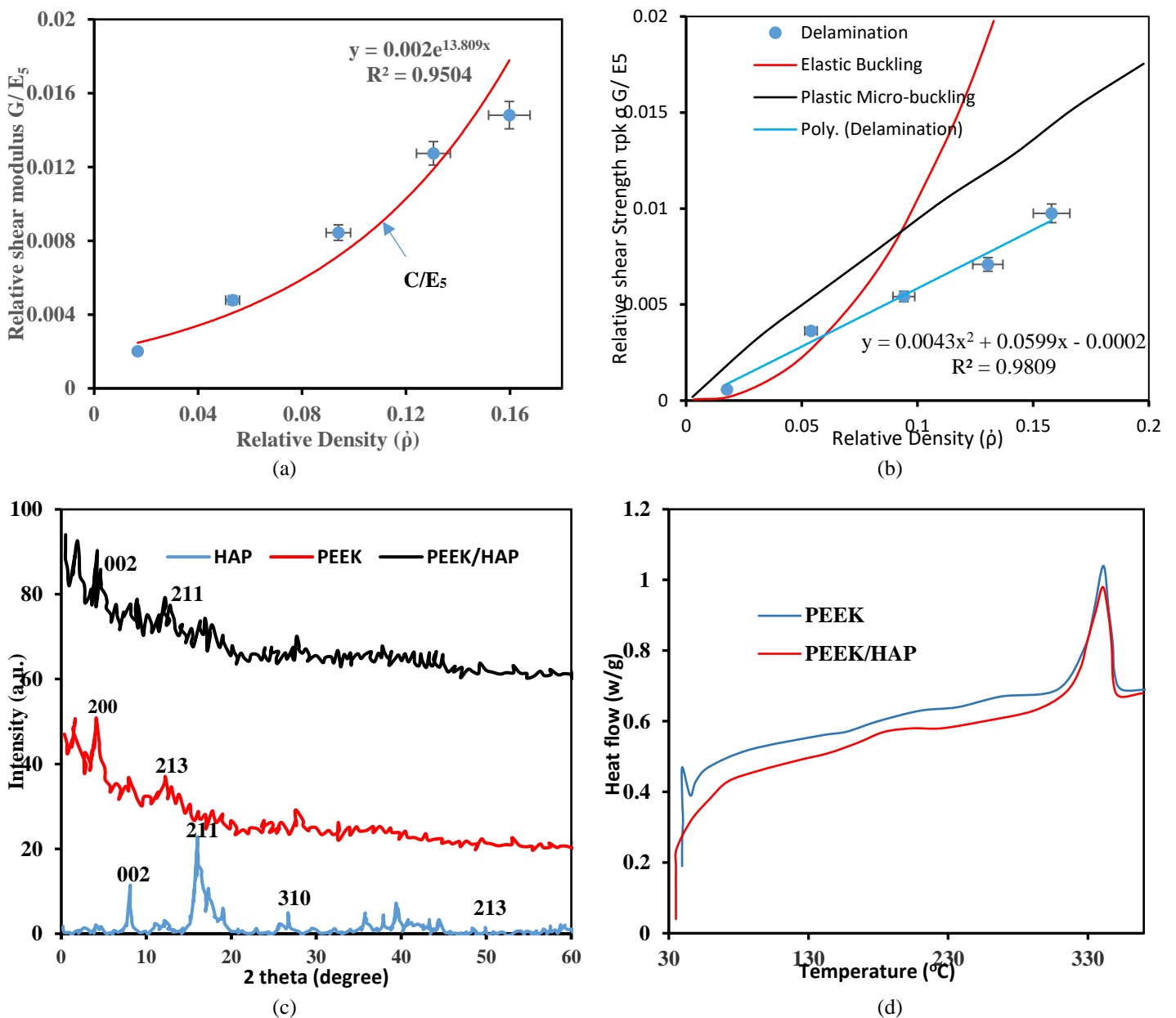


Fig. 7. 3D-printed lattice structure for PEEK composite used for the bone-implant for comparison between measured (a) in-plane relative shear modulus and (b) strengths of the snap-fit cells, as a function of the relative density. Error bars represent the maximum and minimum values obtained from separate measurements. (c) X-ray diffraction spectra for cHAP, PEEK, and PEEK with treatment and (d) DSC curve for the specimen

subjected to thermal shock - side exposed to the treatment.

Furthermore, Fig. 8(a) shows PEEK specimens as-fabricated before and after the tensile test, with detail of the rupture zone. Statically, 3 points of injection fabricated PEEK test body was also the tested inflection, to raise the standard stress-strain curve, as previously presented in Fig. 8a depicts the in-vitro degradation of PEEK molecular weights of neat PEEK/cHAp composites. This was extensively and subsequently elucidated. The result of the complexity against the scaling analysis of the nanoparticle is shown in Figs. 8(b-c), as scale-sensitive fractal analysis of the nanoparticle luminance of the PEEK and fractal analysis of the luminance of the number of grains enclosing box to the scale of the study and (d) failure analysis of the microstructure (Fig. 7d). Summarily, all the results depicted a progressive increase with the number of days.

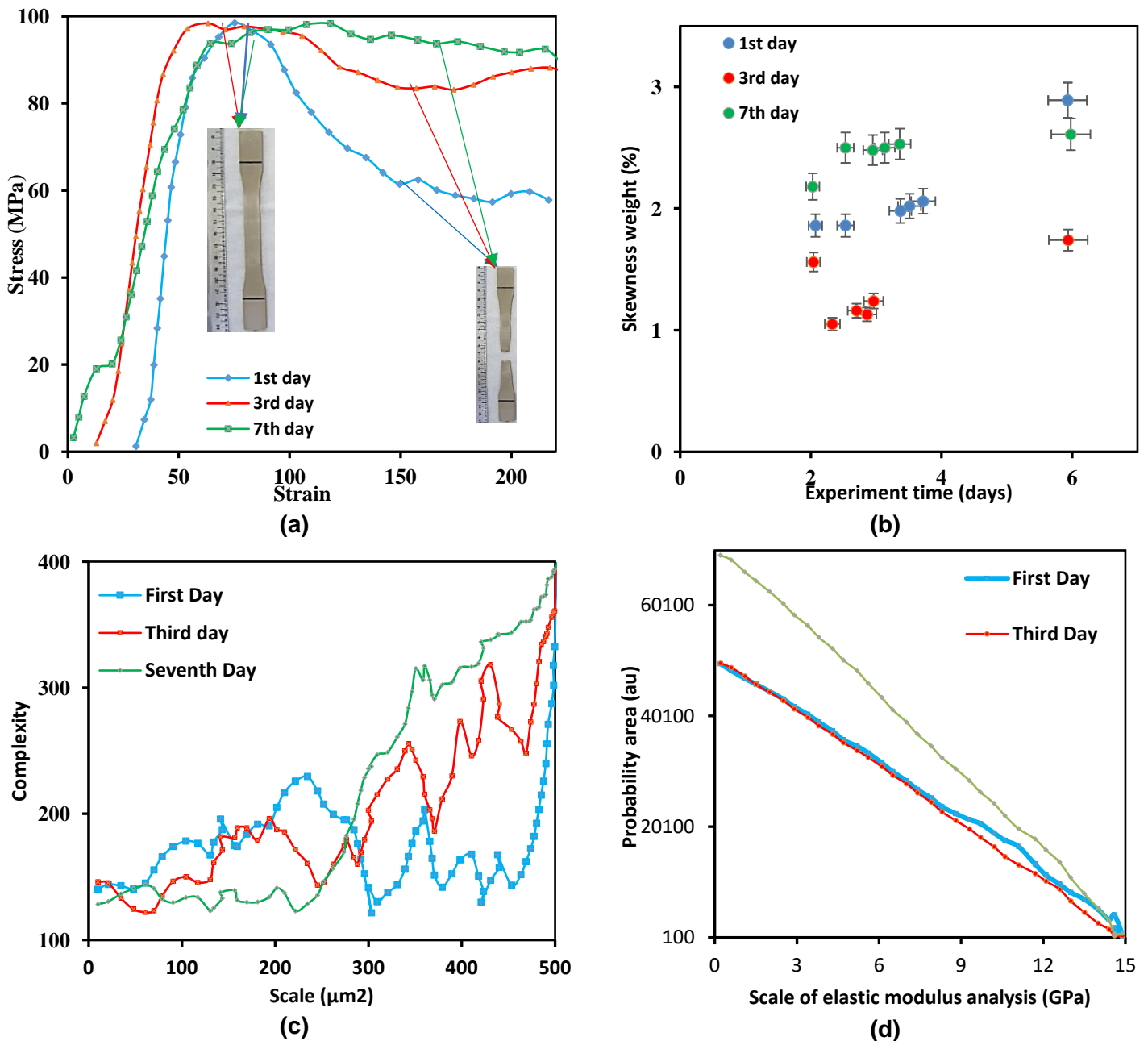
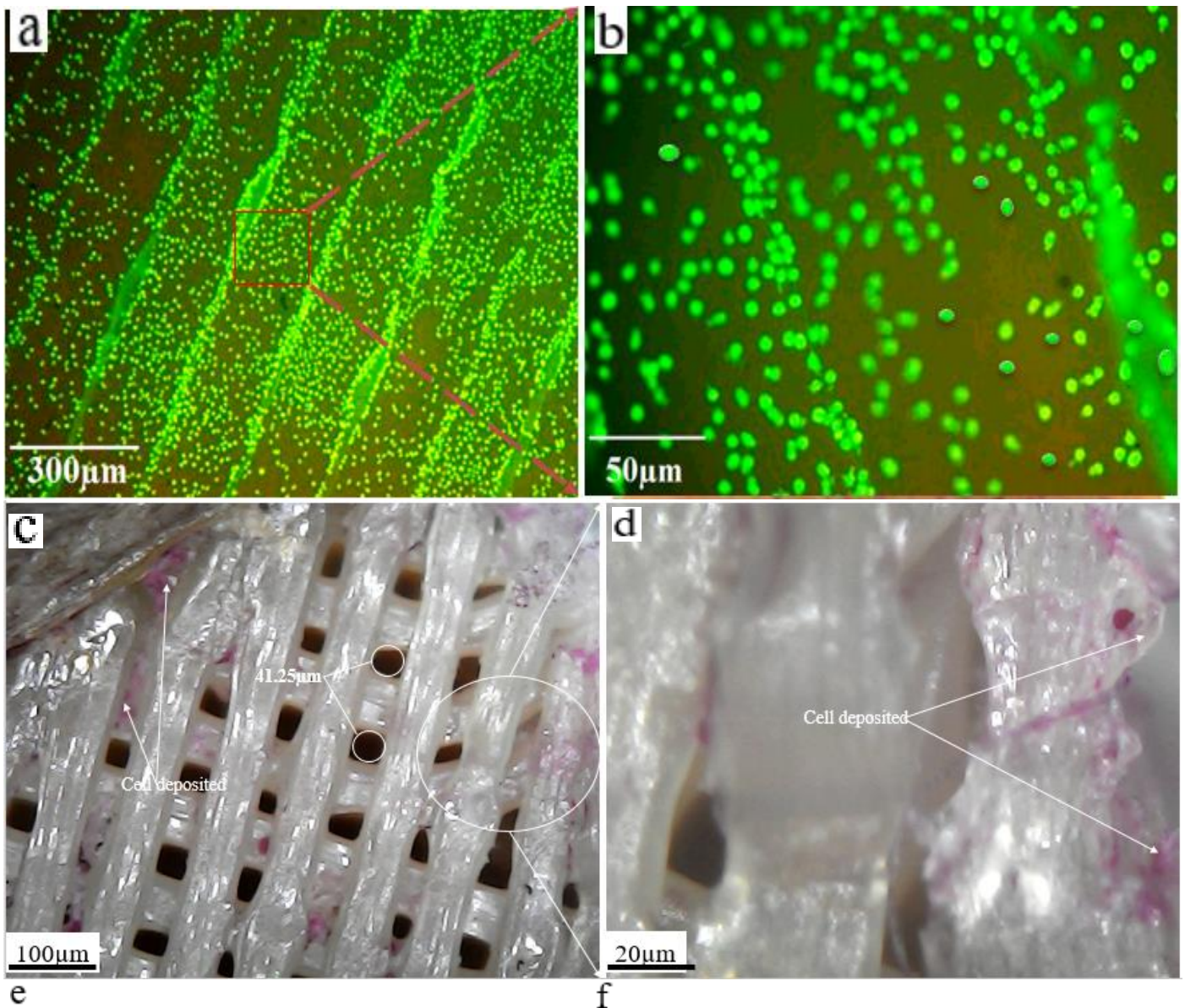


Fig. 8. Scale-sensitive fractal analysis of the nanoparticle luminance of the PEEK composite, showing the (a) compressive stress-strain plot for PEEK/cHAp composites before and after one million cyclic loadings, (b) in-vitro

degradation of PEEK molecular weights of neat PEEK/cHAp composites, (c) fractal analysis of the luminance of the number of grains enclosing box to the scale of the study and (d) failure analysis of the microstructure.

4.2. In-vitro cytotoxicity results

As shown in Fig. 9, the build-up of cells was seen in the surface profile, resulting from the mutual manufacturing process of the deposition layers. The cells in the PEEK/cHAp composite join and formed a cluster, but the cells in the PEEK were dispersed. More prominent actin filaments that bonded adjacent cells were observed in PEEK/cHAp composite. Also, the cell nuclei in the PEEK/cHAp compound were denser than the cell nuclei on the PEEK surfaces. The qualitative and quantitative results of the alkaline phosphatase activity are depicted in Figs. 9 (c) and (d).



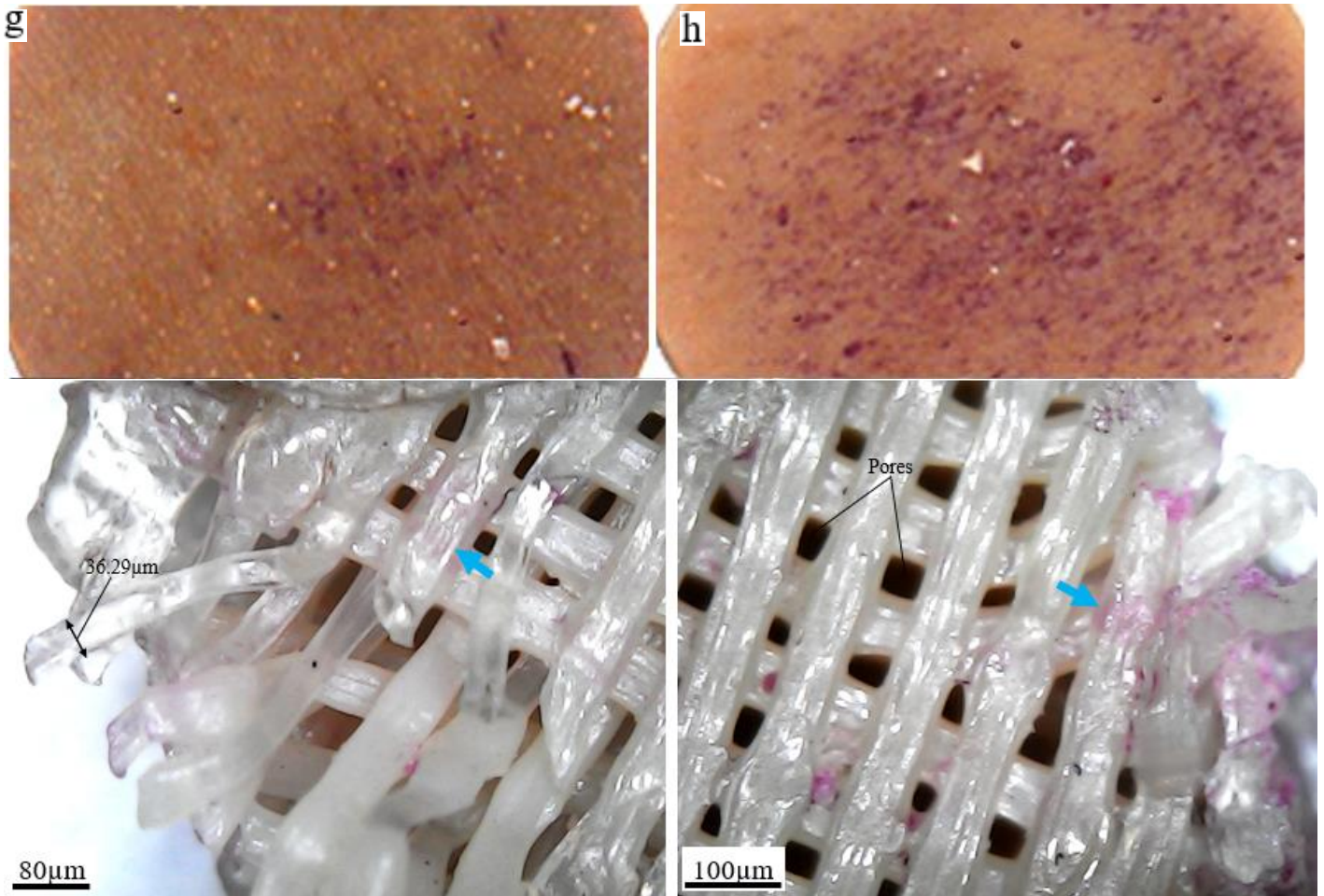


Fig. 9. Cells attached to PEEK and PEEK/cHAp composite scaffold surfaces after culturing for days, showing: (a) 50x magnification, (b) 200x magnification, (c) 100µm of the with the pore of 41.25µm (d) the corresponding magnification of 20µm of cell deposition (e-f) spreading and alkaline phosphatase activity of cells when staining with different material surfaces after 14 days of PEEK and PEEK/cHAp (g-h) Fracture after test showing pores and strang dimension and the cell attachment.

Moreover, the results depict a continuous drop in the values of the E' for all samples after mechanical cycling, as a function of the number of cycles. This effect was corroborated by the results of the drop in the residual stress of the samples at the mechanical fatigue test inflection points. However, there was a significant difference by checking the influence of aging under fatigue on the E'' property and its consequent effect on the $\tan \delta$. There was a decline in the values obtained for E'' with a consequent decrease in $\tan \delta$ for the sample subjected to the thermal shock of the surface coat process, indicating a more elastic response. The fall in $\tan \delta$ value can be attributed to the results effect of the process of strain hardening [56-58], with mechanical cycling for samples subjected to the thermal shock of the surface coat process, as observed from the SEM images of the polymer micro fibrillation on the cryofractured surface. In the samples with effectively coated cHAp, there was an increase in the values of E'' and $\tan \delta$ with aging, indicating a more vicious behavior. This behavior demonstrated that the cHAp particles underwent a detachment from the polymer surface, and as a result, it covered the effect of strain hardening due to the mechanical cycling. Consequently, the thermal-dynamic mechanical analysis allowed the detection of the loss

of interfacial adhesion between the cHAp layer and the PEEK surface.

The final evaluation of the surface coating process concerning the durability under mechanical fatigue of the PEEK coated with cHAp was undefined within the scope of this study. This was because none of the three treatment conditions of the PEEK effectively led to failure, due to the rupture of the specimens in terms of tests of up to one million cycles, even when performed at high strain levels of 85% of the flexed flow point of the evaluated samples. Also, the higher values of residual stress under fatigue obtained for the coated PEEK samples, as well as the lower stress relaxation rate of the same in relation to the samples submitted only to thermal shock and only as fabricated, were clear indications that the surface coat treatment of PEEK with cHAp contributed insignificantly to the deterioration in the mechanical strength of the PEEK, under the fatigue test conditions. Hence, it can contribute to a faster osteointegration in bone tissue engineering applications such as surgical implants.

5. Conclusions

PEEK/cHAp biocomposites have been fabricated using FDM technique in AM process. The biological activities of the composite scaffolds were improved by adding cHAp particles to the PEEK matrix. The tensile properties and elastic moduli of the PEEK/cHAp composites with different cHAp contents, ranging from 0 to 20 wt%, were evaluated. The 15 wt% cHAp exhibited the ideal or optimum percentage weight. In-vitro assays showed that the PEEK/cHAp composite recorded better adhesion, proliferation, spread, and higher alkaline phosphatase activity than pure PEEK. Also, the PEEK/cHAp composite induced the formation of apatite after immersion in the simulated body fluid of DMEM for 14 days. In-vivo results depicted that the osseointegration activity around the PEEK/cHAp composite was higher than that of PEEK. All these results confirmed that after uptake of cHAp, the biological activity of PEEK and its osteogenesis were significantly improved.

Also, the comparative evaluation before and after the mechanical cycling of the $\tan \delta$ values of the cHAp-coated PEEK sample and the sample subjected to thermal shock demonstrated that the DMA analysis identified the deterioration of the interfacial adhesion of the cHAp layer, with the mechanical cycling under fatigue. The fatigue tests under flexion in controlled deformation of 85% at the yield point demonstrated that the stress relaxation, as a function of the mechanical cycling time, occurred at PEEK of -1.58 less than PEEK/cHAp of -1.38. With this order, it was concluded that the main effect on the stress relaxation rate under fatigue could be attributed to the increase in the degree of surface crystallinity and accumulation of residual thermal stresses induced by thermal shock in the PEEK mold. The most significant decrease in the rate of the cHAp-coated PEEK can be traced to the deterioration of the interfacial adhesion of the coating under mechanical fatigue. The tensile test indicated that the surface coating shock significantly reduced the deformation in the rupture of the PEEK/cHAp, as a detailed analysis of the fracture mechanics was carried out. Finally, the limitation identified within this study involves obtaining Wöhler curves of fatigue life of the same materials investigated in a more critical fatigue condition, under controlled deformation. Also, the performing J-integral tests would be useful to identify the degree of reliability of this process for PEEK osteointegration.

References

- [1] Z. Rasheva, G. Zhang, T.A. Burkhart, Correlation between the tribological and mechanical properties of short carbon fibers reinforced PEEK materials with different fiber orientations, *Tribol. Int.* 43 (2010) 1430–1437.
- [2] E.R. Abouzeid, R. Khiari, A. Salama, M. Diab, A. Dufresne, In situ mineralization of nano-hydroxyapatite on bifunctional cellulose nanofiber/polyvinyl alcohol/sodium alginate hydrogel using 3D printing, *Inter. J. Biol. Macromol.* 1601 (2020) 538-547.
- [3] N.T. Evans, F.B. Torstrick, C.S.D. Lee, K.M. Dupont, D.L. Safranski, W.A. Chang, et al., High-strength, surface-porous polyether-ether-ketone for load-bearing orthopedic implants, *Acta Biomater.* 13 (2015) 159–167.
- [4] B.I. Oladapo, A.O.M. Adeoye, M. Ismail, Analytical optimisation of a nanoparticle of microstructural fused deposition of resins for additive manufacturing, *Compos. Part B Eng.* 150 (2018) 248-254.
- [5] L. Li, S. Qin, J. Peng, A. Chen, K. Song, Engineering gelatin-based alginate/carbon nanotubes blend bioink for direct 3D printing of vessel constructs, *Inter. J. Biol. Macromol.* 14515 (2020) 262-271.
- [6] C.O. Ijagbemi, B.I. Oladapo, H.M. Campbell, C.O. Ijagbemi, Design and simulation of fatigue analysis for a vehicle suspension system (VSS) and its effect on global warming, *Proc. Eng.* 159 (2016) 124-132.
- [7] Y. Liu, R. Wang, S. Chen, Z. Xu, J. Chen, Heparan sulfate loaded polycaprolactone-hydroxyapatite scaffolds with 3D printing for bone defect repair, *Inter. J. Biol. Macromol.* 1481 (2020) 153-162.
- [8] A.O.M. Adeoye, J.F. Kayode, B.I. Oladapo, S.O. Afolabi, Experimental analysis and optimization of synthesized magnetic nanoparticles coated with PMAMPC-MNPs for bioengineering application, *St. Petersburg Polytech. Univ. J. Phys. Math.* 3 (2017) 333-338.
- [9] T.P. Oliveira, S.N. Silva, J.A. Sousa, Flexural fatigue behavior of hydroxyapatite-coated polyether-ether-ketone (PEEK) injection moldings derived from dynamic mechanical analysis, *Inter. J. Fatig.* 108 (2018) 1-8.
- [10] Z. Khurshid, M. Zafar, S. Qasim, S. Shahab, M. Naseem, A. AbuReqaiba, Advances in nanotechnology for restorative dentistry, *Materials* 8 (2015) 717-731.
- [11] B.C. Maniglia, D.C. Lima, M.D. Matta Junior, P. Le-Bail, P.E.D. Augusto, Hydrogels based on ozonated cassava starch: Effect of ozone processing and gelatinization conditions on enhancing 3D-printing applications, *Inter. J. Biol. Macromol.* 1381 (2019) 1087-1097.
- [12] M.H. Abdulkareema, A.H. Abdalsalam, A.J. Bohan, Influence of chitosan on the antibacterial activity of composite coating (PEEK/cHAp) fabricated by electrophoretic deposition, *Prog. Org. Coat.* 130 (2019) 251-259.
- [13] M.J. Kadhim, N.E. Abdullatef, M.H. Abdulkareem, Optimization of nanohydroxyapatite/chitosan electrophoretic deposition on 316L stainless steel using taguchi design of experiments, *Al-Nahrain J. Eng. Sci.* 20 (2017) 1215-1227.
- [14] S. Najeeb, M.S. Zafar, Z. Khurshid, F. Siddiqui, Applications of polyetheretherketone (PEEK) in oral implantology and prosthodontics, *J. Prosthodontics.* 60 (2016) 12-19.
- [15] T.H.C.M.A. Song, Y.W. Lee, Characterization of an inductively coupled nitrogen-argon surface coat by Langmuir probe combined with optical emission spectroscopy, *Phys. Plasmas*, 18 (2011) 023504.

- [16] J. Waser-Althaus, A. Salamon, M. Waser, C. Padeste, M. Kreutzer, U. Pieleles, et al., Differentiation of human mesenchymal stem cells on plasma-treated polyetheretherketone, *J. Mater. Sci. Mater. Med.* 25 (2014) 515-525.
- [17] B.I. Oladapo, S.A. Zahedi, A.O.M. Adeoye, 3D printing of bone scaffolds with hybrid biomaterials, *Compos. Part B Eng.* 158 (2019) 428-436.
- [18] E. Ilhan, S. Cesur, E. Guler, F. Topal, O. Gunduz, Development of *Satureja cuneifolia*-loaded sodium alginate/polyethylene glycol scaffolds produced by 3D-printing technology as a diabetic wound dressing material, *Inter. J. Biol. Macromol.* 16115 (2020) 1040-1054.
- [19] B.I. Oladapo, S.A. Zahedi, F. Vahidnia, O.M. Ikumapayi, M.U. Farooq, Three-dimensional finite element analysis of a porcelain crowned tooth, *Beni-Suef Univ. J. Basic Appl. Sci.* 7 (2019) 461-464.
- [20] B. Stawarczyk, M. Eichberger, J. Uhrenbacher, T. Wimmer, D. Edelhoff, P.R. Schmidlin, Three-unit reinforced poly ether ether ketone composite FDPs: Influence of fabrication method on load-bearing capacity and failure types, *Dent. Mater. J.* 34 (2015) 7-12.
- [21] L. Tytgat, L.V. Damme, M.P.O. Arevalo, H. Declercq, S.V. Vlierberghe, Extrusion-based 3D printing of photo-crosslinkable gelatin and κ -carrageenan hydrogel blends for adipose tissue regeneration, *Inter. J. Biol. Macromol.* 1401 (2019) 929-938.
- [22] B.I. Oladapo, S.A. Zahedi, S.C. Chaluvadi, S.S. Bollapalli, M. Ismail, Model design of a superconducting quantum interference device of magnetic field sensors for magnetocardiography, *Biomed. Sig. Proc. Cont.* 46 (2019) 116-120.
- [23] B. Ashwin, B. Abinaya, T. P. Prasith, S. Viji Chandran, N. Selvamurugan, 3D-poly (lactic acid) scaffolds coated with gelatin and mucic acid for bone tissue engineering, *Inter. J. Biol. Macromol.* 1621 (2020) 523-532.
- [24] B.I. Oladapo, S.A. Zahedi, F.T. Omigbodun, E.A. Oshin, V.A. Adebisi, O.B. Malachi, Microstructural evaluation of aluminium alloy A365 T6 in machining operation, *J. Mater. Res. Technol.* 8 (2019) 3213-3222.
- [25] S. Najeeb, Z. Khurshid, J.P. Matinlinna, F. Siddiqui, M.Z. Nassani, K. Baroudi, Nanomodified peek dental implants: Bioactive composites and surface modification - A review, *Int. J. Dent.* 2015 (2015) 1-7.
- [26] Y. Zhu, X. Liu, K.W.K. Yeung, P.K. Chu, W. Shuilin, Biofunctionalization of carbon nanotubes/chitosan hybrids on Ti implants by atom layer deposited ZnO nanostructures, *Appl. Surf. Sci.*, 400 (2017) 14-23.
- [27] Z. Liu, M. Zhang, B. Bhandari, Effect of gums on the rheological, microstructural and extrusion printing characteristics of mashed potatoes, *Inter. J. Biol. Macromol.* 1171 (2018) 1179-1187.
- [28] N. Ranjan, R. Singh, I.S. Ahuja, Biocompatible thermoplastic composite blended with cHAp and CS for 3D printing. In: S. Hashmi, I.A. Choudhury (Eds.), *Ref. Mod. Mater. Sci. Mater. Eng., Encycl. Ren. Sust. Mater.* 4 (2020) 379-388.
- [29] M.S. Zafar, N. Ahmed, Nanoindentation and surface roughness profilometry of poly methyl methacrylate denture base materials, *Technol. Health Care* 22 (2014) 573-581.
- [30] F. Kong, Z. Nie, Z. Liu, S. Hou, J. Ji, Developments of nano-TiO₂ incorporated hydroxyapatite/PEEK composite strut for cervical reconstruction and interbody fusion after corpectomy with anterior plate fixation, *J. Photochem. Photobiol. B Biol.* 187 (2018) 120-125.

- [31] M.H. Abdulkareem, A.H. Abdalsalam, A.J. Bohan, Influence of chitosan on the antibacterial activity of composite coating (PEEK/cHAp) fabricated by electrophoretic deposition, *Prog. Org. Coat.* 130 (2019) 251-259.
- [32] J. Chakravarty, M.F. Rabbi, V. Chalivendra, T. Ferreira, C.J. Brigham, Mechanical and biological properties of chitin/poly(lactide (PLA)/hydroxyapatite (HAp) composites cast using ionic liquid solutions, *Inter. J. Biol. Macromol.* 15115 (2020) 1213-1223.
- [33] Zahedi S.A., Demiral M., Roy A., Silberschmidt V.V., (2017) FE/SPH modelling of orthogonal micro-machining of fcc single crystal, *Computational materials science* 78, 104-109
- [34] R.B. Durairaj, P. Borah, Y. Thuvaragees, Characterization of PEEK coated S.S316 1 for biomedical application, *ARPN J. Eng. Appl. Sci.* 10 (2015) 4794 – 4798.
- [35] Zahedi A, Demiral M, Roy A, Babitsky VI, Silberschmidt VV (2012) Indentation in fcc single crystals *Solid State Phenomena* 188: 219-225
- [36] D. Boonyawan, P. Waruriya, K. Suttiat, Characterization of titanium nitride–Hydroxyapatite on PEEK for dental implants by co-axis target magnetron sputtering, *Surf. Coat. Technol.* 306, Part A (2016) 164-170.
- [37] S. Singh, C. Prakash, S. Ramakrishna, 3D printing of polyether-ether-ketone for biomedical applications, *Europ. Polym. J.* 114 (2019) 234-248.
- [38] J. Prakash, D. Prema, K.S. Venkataprasanna, K. Balagangadharan, G.D. Venkatasubbu, Nanocomposite chitosan film containing graphene oxide/hydroxyapatite/gold for bone tissue engineering, *Inter. J. Biol. Macromol.* 1541 (2020) 62-71.
- [39] J.W. Durham III, S.A. Montelongo, J.L. Ong, T. Guda, M.J. Allen, A. Rabiei, Hydroxyapatite coating on PEEK implants: Biomechanical and histological study in a rabbit model, *Mater. Sci. Eng.* 68 (2016) 723-731.
- [40] H. Luo, G. Xiong, K. Ren, S.R. Raman, Y. Wan, Air DBD surface coat treatment on three-dimensional braided carbon fiber-reinforced PEEK composites for enhancement of in vitro bioactivity, *Surf. Coat. Technol.* 242 (2014) 1-7.
- [41] D. Almasi, S. Izman, M. Assadian, M. Ghanbari, M.R. Abdul Kadir, Crystalline ha coating on PEEK via chemical deposition, *Appl. Surf. Sci.* 314 (2014) 1034-1040.
- [42] F.T. Omigbodun, B.I. Oladapo, O.K. Bowoto, F.P. Adeyekun, Experimental model design and simulation of air conditioning system for energy management, *Inter. Res. J. Eng. Technol.* 6 (2019) 811-816.
- [43] O. Sproesser, P.R. Schmidlin, J. Uhrenbacher, M. Roos, W. Gernet, B. Stawarczyk, Effect of sulfuric acid etching of polyetheretherketone on the shear bond strength to resin cements, *J. Adhes. Dent.* 16 (2014) 465-472.
- [44] F.T. Omigbodun, B.I. Oladapo, O.K. Bowoto, F.P. Adeyekun, Modelling detection of magnetic hysteresis properties with a microcontroller, *Inter. J. Eng. Trends Technol.* 67 (2019) 5-12.
- [45] V.A. Balogun, B.I. Oladapo, Electrical energy demand modeling of 3D printing technology for sustainable manufacture, *Inter. J. Eng.* 29 (2019) 1-8.
- [46] V. Alt, M. Hannig, B. Wöstmann, M. Balkenhol, the Fracture strength of temporary fixed partial dentures: CAD/CAM versus directly fabricated restorations, *Dental Mater.* 27 (2011) 339-347.

- [47] Shamsi-Sarband A., Zahedi S. A., Bakhshi-Jouybari M., Hossinipour S. J., Banabic D. (2012) Optimization of the pressure path in sheet metal hydroforming, *Journal Proceedings Of The Romanian Academy*, A 13: 351-359
- [48] D. Huang, X. Du, H. Liang, W. Hu, H. Hu, X. Cheng, Anterior corpectomy versus posterior laminoplasty for the treatment of multilevel cervical myelopathy: A meta-analysis, *Int. J. Surg.* 35 (2016) 21-27.
- [49] S. Wu, Z. Weng, X. Liu, K.W.K. Yeung, P.K. Chu, Functionalized TiO₂ based nanomaterials for biomedical applications, *Adv. Funct. Mater.* 24 (2014) 5464-5481.
- [50] Li S., Zahedi SA., Silberschmidt V., (2017), Numerical Simulation of Bone Cutting: Hybrid SPH-FE Approach Numerical Methods and Advanced Simulation in Biomechanics and Biological Processes, 187-201
- [51] V. Azar, B. Hashemi, M.R. Yazdi, The effect of shot peening on fatigue and corrosion behavior of 316L stainless steel in Ringer's solution, *Surf. Coat. Technol.*, 204 (2010) 3546-3551.
- [52] K. Kandiah, P. Muthusamy, S. Mohan, R., Venkatachalam, TiO₂-graphene nanocomposites for enhanced osteocalcin induction, *Mater. Sci. Eng.* 38 (2014) 252-262.
- [53] Q. Chen, Y. Liu, Q.Q. Yao, S.S. Yu, K. Zheng, M. Pischetsrieder, et al., Multi layered bioactive composite coating drug delivery capability by electrophoretic deposition combined with layer-by-layer deposition, *Adv. Biomater. Devices Med.*, I (2014) 18-27.
- [54] Y. Torres, C. Romero, Q. Chen, G. Pérez, J.A. Rodríguez-Ortiz, J.J. Pavón, et al., Electrophoretic deposition of PEEK/45S5 bioactive glass coating on porous titanium substrate: Influence of processing conditions and porosity parameters, *Key Eng. Mater.* 704 (2016) 343-350.
- [55] Tafaoli-Masoule M, Shakeri M, Zahedi SA, Seitz H, Vaezi M (2019) 3D printing of PEEK-based medical devices *Transactions on Additive Manufacturing Meets Medicine* 1 (1)
- [56] Z. Liu, Y. Zhu, X. Liu, K.W.K. Yeung, S. Wu, Construction of poly (vinyl alcohol)/poly(lactide-glycolide acid)/vancomycin nanoparticles on titanium for enhancing the surface self-antibacterial activity and cytocompatibility, *Colloids Surf. B Biointerf.* 151 (2017) 165-177.
- [57] H.S. Ragab, F.A. Ibrahim, F. Abdallah, A.A. Al-Ghamdi, F. El-Tantawy, N. Radwan, et al., Synthesis and in vitro antibacterial properties of hydroxyapatite nanoparticles. *IOSR J. Pharm. Biol. Sci.* 9 (2014) 77-85.
- [58] B. Stawarczyk, A. Ender, A. Trottmann, M. Özcan, J. Fischer, C.H. Hämmerle, Load-bearing capacity of CAD/CAM milled polymeric three-unit fixed dental prostheses: Effect of aging regimens, *Clin. Oral Invest.* 16 (2012) 1669-1677.